Validation of Theoretical Methods for the Structure and Energy of Aluminum Clusters

Nathan E. Schultz, Grażyna Staszewska,† Przemysław Staszewski,‡ and Donald G. Truhlar*

Department of Chemistry and Supercomputer Institute, University of Minnesota, Minneapolis, Minnesota 55455-0431

Received: October 7, 2003; In Final Form: December 12, 2003

We calculated the atomization energy of aluminum clusters (Al_2−Al_7) with several multilevel methods, including MCG3/3 and G3X, that have been previously shown to provide high accuracy for atomization energies. We used the results to test a number of hybrid density functional theory (HDFT) methods and found that the PBE0 method is in best agreement with the accurate methods. We then used the PBE0/MG3 method to develop a more extensive data set for the energies of small aluminum clusters (Al_2−Al_{13}), and this was used to test a number of semiempirical methods, in particular Austin model 1 (AM1), modified neglect of differential overlap (MNDO), modified symmetric-orthogonalized intermediate neglect of differential overlap (MSINDO) with and without d-functions, parametrized model 3 (PM3), and the tight-binding total energy (TBTE) method, for geometries, energies, and multiplicities of Al clusters. The AM1 model and MSINDO model are the most accurate of the semiempirical methods for energetics, and PM3 is the most accurate method for geometries.

1. Introduction

The formation of Al_3O_2(s) is highly exothermic (−200 kcal/mol);[1] thus aluminum, in principle, makes an excellent high-energy fuel, and there is a considerable interest in understanding the kinetics of aluminum oxidation, especially for aluminum nanoparticles. In a more general context, because nanostructured materials can have many properties that differ from the bulk material,[2−7] there is great interest in developing theoretical models to predict the properties of nanoparticles. It is difficult to assess which computational methods are most appropriate for nanoaluminum because there is limited experimental data for neutral clusters, and the available data are limited to very small clusters (Al_2 and Al_3)[8−10] on one hand and bulk aluminum on the other hand. The boundary between small clusters and nanoparticles (diameter > 1 nm) occurs around Al_{40}. In the present paper we study clusters with diameters up to 0.7 nm, as a first step toward developing methods suitable for nanoparticles.

Multilevel calculations involve the combination of different methods of treating electron correlation in electronic structure theory and/or different one-electron basis sets to attempt to extrapolate toward a result that is more accurate than the most sophisticated single-level calculations.[11−39] Multicoefficient correlation methods (MCCMs), which use linear combinations of scaled energy components, are a particularly efficient type of multilevel method.[23−26,28,30,32,35,36,39] The most recent suite of MCCM methods is denoted version 3 (MCCM/3),[39] and the most accurate method in the MCCM/3 suite is version 3 of the multicoefficient Gaussian-3 (MCG3/3) method.[25,26] However, the method has a component whose computation time scales as N,[7] where N is the number of atoms. The computer time that is required for an MCG3/3 calculation would be prohibitively expensive for large systems; therefore we need to find a method that is comparable in accuracy to an MCG3/3 calculation but is considerably less expensive. The more computationally tractable multilevel methods in the MCCM/3 suite of methods are MC-QCISD/3,[23,39] MC-Utah/3 (MC-UT/3),[23,39] and MC-Colorado/3 (MC-CO/3).[23,39] MC-QCISD/3 and MC-UT/3 both have components that scale as N,[6] and MC-CO/3 has components that scale as N.[5]

Gaussian-3 theory[19] (G3) is another type of multilevel calculation, and in this method the semiempirical character is expressed by four additive correction terms whose sum is called the high-level correction (HLC). The Gaussian-3 extended (G3X) method[35] is a more accurate, and more computationally expensive, variation of G3 theory. The G3 and G3X methods also have steps that scale as N.[7]

The computational effort for hybrid density functional theory[40−45] (HDFT), which is a hybrid of Hartree−Fock theory and gradient-corrected density functional theory, scales as N.[4] Because HDFT is a very cost-effective method, we will survey a variety of HDFT methods with different basis sets to determine which HDFT method agrees best with MCG3/3 and G3X. The HDFT methods that we will test are B3LYP,[40,41] mPW1PW91,[43] MPW1K,[45] and PBE0,[44,46,47] each with the 6-31+G(d)[48−50] and the MG3[19,25,48−52] basis sets. (For Al, the MG3 basis set is the 6-311+G(3d2f) basis[51] and is also called G3Large-MP2[22]).

There have been several previous theoretical studies of Al_3−Al_7.[5,53−56] An important finding in these studies is that there are multiple possible structures for each cluster size, including both symmetric and nonsymmetric structures. Furthermore, each structure has a manifold of nearly degenerate multiplicities and electronic states. In light of these findings we will develop a large data set with considerable structural diversity. We have adopted a boot-strap philosophy in our investigations. We will

† Permanent address: Institute of Physics, Nicholas Copernicus University, ul. Grudziądska 5, 87-100 Toruń, Poland.

‡ Permanent address: Department of Theoretical Foundations of Biomedical Science and Medical Informatics, Ludwik-Rydygier Medical University, ul. Jagiellońska 13, 85−067 Bydgoszcz, Poland.

10.1021/jp0370223 CCC: $27.50
Published on Web 03/24/2004

first develop a small data set with our most accurate method. This data set will then be used to validate a cost-effective method, which we will use to develop a larger data set. The goal is to determine an accurate quantum-mechanical method that can treat aluminum clusters that range in size from Al_2−Al_{13}. Then we will use this to develop a data set to test methods that can be applied more economically to actual nanoparticles. Treatment of a cluster at least as large as Al_{13} is necessary to obtain a representative data set because it is the first cluster size that has an atom coordinated to 12 others, which is the coordination state of bulk aluminum and hence also the state of many of the interior atoms in larger nanoparticles.

We will first examine Al_2 and Al_3 with MCG3/3 and G3X in an attempt to determine which one (if either) is more accurate. Then we will develop the small Al data set and validate a less expensive method to develop the larger data set for testing neglect of differential overlap (NDO) and tight binding (TB) methods. The NDO methods that we will examine are modified neglect of differential overlap (MNDO),[57,58] Austin model 1 (AM1),[59,60] parametrized method 3 (PM3),[61] modified symmetric-orthogonalized intermediate neglect of differential overlap (MSINDO)[62,63] with d-functions, and MSINDO[62,63] without d-functions (we will denote MSINDO without d-functions as MSINDO/xd), and the TB method is tight-binding total energy (TBTE).[64−66] The AM1, MNDO, MSINDO, MSINDO/xd, and PM3 methods are self-consistent field (SCF) methods, whereas TBTE is a nonorthogonal, noniterative tight binding method,[67,68] which is considerably less expensive. (Tight-binding methods are also called extended Hückel theory.) We will also find that, for understanding some of the trends, we need to use a nonclose subset of the large data set, i.e., a subset with no close approaches of any two atoms.

2. Description of the Multilevel Calculations

Details of the G3X[35,36] and MCCM/3[39] methods have been given elsewhere, but we will briefly summarize the methods here and focus on their differences. Levels of electron correlation that are used in one or more of the multilevel methods are second-, third-, and fourth-order Møller−Plesset perturbation theory,[69] denoted MP2, MP3, and MP4, respectively, fourth-order perturbation theory without the computationally demanding triples contribution, denoted as MP4SDQ, and quadratic configuration interaction with single and double substitutions and quasi-perturbative triples,[70] denoted QCISD(T). These methods all constrain the core orbitals to remain doubly occupied; the G3X method also uses the MP2(full) method, where the core orbitals are not forced to maintain double occupancy. The MCCM/3 methods were parametrized with geometries obtained by the QCISD level of theory with the MG3 basis set, but that is not an intrinsic part of the method; the MCCM/3 methods may be used with any good geometry, or the methods may also be used to optimize geometries.[71] G3X, however, is *defined* as using specific geometries; for Al compounds these are B3LYP/6-31G(2df) geometries.[36]

The equation for the high-level correction (HLC) in the G3X method is

$$E(\mathrm{HLC}) = -An_\beta - B(n_\alpha - n_\beta) \quad (1)$$

where n_β and n_α are the number of β and α electrons, respectively, with $n_\alpha > n_\beta$, and the parameters A and B are empirical parameters, with different values for atoms and molecules. The total zero-point exclusive G3X energy is

$$E(\mathrm{G3X}) = E(\mathrm{MP4/d}) + E(\mathrm{QCISD(T)/d - MP4/d}) + E(\mathrm{MP4/diff - MP4/d}) + E(\mathrm{MP4/2df,p - MP4/d - MP2/diff + MP2/d}) + E(\mathrm{MP2(full)/G3L - MP2/2df,p - MP2/diff + MP2/d}) + E(\mathrm{HF/G3XL - HF/G3L}) + E(\mathrm{SO}) \quad (2)$$

where d denotes 6-31G(d), diff denotes 6-31+G(d), 2df,p denotes 6-31G(2df,p), G3L denotes the G3Large basis set,[70] G3XL denotes the G3XLarge basis set,[36] and E(SO) is a spin−orbit correction for atoms and is taken from experiment.[72] The G3Large basis set is equivalent to the MG3 basis set except that G3Large contains core-polarization functions. The G3XLarge is the G3Large basis set extended by a set of valence g-polarization functions for second-row elements.

The energy expressions for the MCCM/3 methods are

$$E(\mathrm{MC\text{-}CO/3}) = E(\mathrm{HF/2d}) + c_1E(\mathrm{HF/MG3S - HF/2d}) + c_2E(\mathrm{MP2/2d - HF/2d}) + c_3E(\mathrm{MP2/MG3S - MP2/2d - HF/MG3S + HF/2d}) + E(\mathrm{SO}) \quad (3)$$

$$E(\mathrm{MC\text{-}UT/3}) = E(\mathrm{HF/d}) + c_1E(\mathrm{HF/MG3S - HF/d}) + c_2E(\mathrm{MP2/d - HF/d}) + c_3E(\mathrm{MP2/MG3S - MP2/d - HF/MG3S + HF/d}) + c_4E(\mathrm{MP4SDQ/d - MP2/d}) + E(\mathrm{SO}) \quad (4)$$

$$E(\mathrm{MC\text{-}QCISD/3}) = E(\mathrm{HF/d}) + c_1E(\mathrm{HF/MG3S - HF/d}) + c_2E(\mathrm{MP2/d - HF/d}) + c_3E(\mathrm{MP2/MG3S - MP2/d - HF/MG3S + HF/d}) + c_4E(\mathrm{QCISD(T)/d - MP2/d}) + E(\mathrm{SO}) \quad (5)$$

$$E(\mathrm{MCG3/3}) = c_0E(\mathrm{HF/d}) + c_1E(\mathrm{HF/MG3S - HF/d}) + c_2E(\mathrm{MP2/d - HF/d}) + c_3E(\mathrm{MP2/MG3S - MP2/d - HF/MG3S + HF/d}) + c_4E(\mathrm{MP4SDQ/d - MP2/d}) + c_5E(\mathrm{MP4SDQ/T\text{-}2df - MP4SDQ/d - MP2/T\text{-}2df + MP2/d}) + c_6E(\mathrm{QCISD(T)/d - MP4SDQ/d}) + E(\mathrm{SO}) \quad (6)$$

where 2d denotes 6-31G(2d), T-2df denotes 6-311G(2df,p), MG3S is the MG3 basis set for all elements except H, for which the diffuse functions have been removed, and the c_i are method-dependent multiplicative scale factors. The c_0 coefficient has been set equal to 1 if it is not present in an equation.

3. Small Al Data Set

Our small Al data set contains the atomization energies of Al_2, Al_3, and Al_4 plus two Al_6 and two Al_7 clusters (see Figure 1). We used the lowest-energy structures of Al_2, Al_3, Al_4, and Al_6. The ground state of Al_4 is a planar rhombus[54,56] and not a three-dimensional tetrahedron. The smallest aluminum cluster that has a three-dimensional ground state is Al_6, which has an octahedral ground state.[54] This structure is in our data set and is called Al_6(opt), because it is an optimized octahedron. The other Al_6 structure is called Al_6(bulk), and it is an octahedron with the bulk bond length of 2.8635 Å, which is obtained by dividing the experimental (298 K) lattice constant, 4.04964 Å,[73] by $\sqrt{2}$. One structure for Al_7 is the ground state with C_s symmetry, and it is called $Al_7(C_s)$. It is best described as an octahedron with an aluminum atom on a 3-fold face. The second structure for Al_7 is an octahedron that has one interior atom surrounded by 6 surface atoms. This structure, called $Al_7(O_h)$,

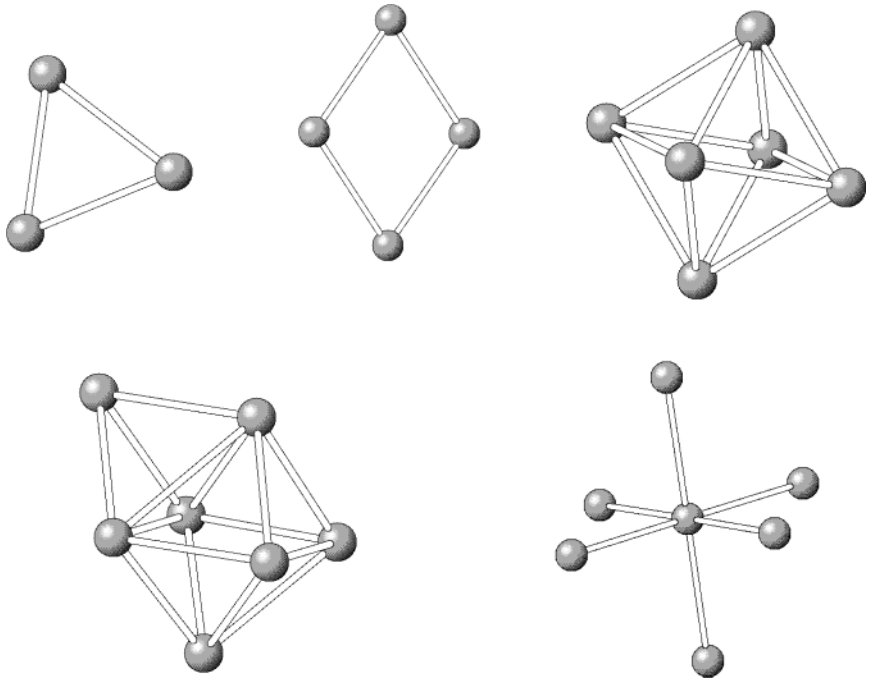

Figure 1. Optimized structures for the small aluminum training set with two or more atoms.

may be considered a model nanoparticle, because it has both surface and interior atoms.

4. Results and Discussion

The HDFT and multilevel calculations were performed with *Gaussian*98.[74] The linear combinations in the MCCM/3 and G3X calculations can be automated with the MULTILEVEL[75] program. The AM1, MNDO, and PM3 calculations were performed with the mopac 5.09mn program,[76] except for clusters that were larger than Al_{13}, which were calculated with *Gaussian*03[77] because the SCF calculations showed better convergence. The MSINDO and MSINDO/xd calculations were performed with the MSINDO[78] program. All of the clusters in the present paper have open-shell electronic structures, and the calculations were carried out using the spin-unrestricted formalism (except for the tight-binding calculations).[79] The tight-binding calculations were performed with the static[80] computer program from the Naval Research Laboratory (http://cst-www.nrl.navy.mil/bind/static/index.html). Throughout the article, for each geometry and each method, we found the lowest energy from among all the possible state symmetries and spin states, i.e., from among all the possible orbital occupancy patterns and multiplicities. Thus, when comparing energies, we are comparing the ground-state energies predicted by each method, although they sometimes correspond to different states.

4.1. Al_2 and Al_3. As mentioned in section 2, the multilevel methods may be used to optimize geometries; however, this would be cost prohibitive for large systems, and it is only done here for Al_2 and Al_3. Thus a comprehensive study of Al_2 and Al_3 was conducted to determine a suitable method for geometry optimizations. Table 1 compares the bond lengths of Al_2 and Al_3 with a variety of computational methods. The only method in Table 1 that has not been previously discussed is coupled-cluster theory with single and double excitations and perturbative triples, denoted CCSD(T),[81−83] with the MG3 basis set. The CCSD(T)/MG3 calculations were included, because the CCSD(T) method with a large basis is known to yield accurate atomization energies,[84] although not as accurate as methods such as MCG3/3 and G3X, unless one extrapolates to a complete basis set.[39]

TABLE 1: Optimized Bond Lengths (Å) for Al_2 ($^3\Pi_u$) and Al_3 ($^2A_1'$) and Mean Unsigned Deviation from MCG3/3

	Al_2	Al_3[a]	MUE[b]
B3LYP/6-31G(2df)[c]	2.753	2.536	0.028
B3LYP/6-31+G(d)	2.764	2.544	0.038
B3LYP/MG3	2.752	2.531	0.025
CCSD(T)/6-31+G(d)	2.708	2.537	0.007
CCSD(T)/MG3	2.716	2.529	0.006
MCG3/3[d]	**2.709**	**2.523**	
MP2/6-31+G(d)	2.707	2.592	0.035
MP2/MG3	2.710	2.617	0.047
MPW1K/6-31+G(d)	2.716	2.504	0.013
MPW1K/MG3	2.714	2.500	0.013
mPW1PW91/6-31+G(d)	2.734	2.514	0.017
mPW1PW91/MG3	2.729	2.507	0.018
PBE0/6-31+G(d)	2.734	2.513	0.017
PBE0/MG3	2.730	2.506	0.019
QCISD/6-31+G(d)	2.711	2.533	0.006
QCISD/MG3	2.718	2.531	0.008

[a] The geometry for Al_3 is an equilateral triangle, so all of the bond angles are 60°. [b] Mean unsigned differences from MCG3/3 results. [c] Included because this is the method used to calculate the geometry for aluminum compounds in the standard G3X method. [d] Most accurate method in the table.

All of the methods in Table 1 predict the lowest energy state for Al_2 to be the $^3\Pi_u$ electronic state, which is consistent with previous calculations.[54,56,85,86] The methods also predict the lowest energy state for Al_3 to be the $^2A_1'$ state, which is also consistent with previous calculations.[54−56,85]

Table 1 shows that the CCSD(T)/MG3 and QCISD/6-31+G(d) methods have the best agreement with the geometries predicted by MCG3/3. The mean-unsigned error (MUE), where the error is defined as the difference between the calculated bond length and the bond length calculated with the MCG3/3 method, for CCSD(T)/MG3 and QCISD/6-31+G(d) are both 0.006 Å. The CCSD(T) method, unfortunately, does not have affordable analytical gradients, and thus derivatives with respect to internuclear distances are performed numerically. From the standpoint of practicality, a method used for geometry optimization should have affordable analytical gradients. The QCISD method has affordable analytical gradients, and the 6-31+G(d)

TABLE 2: Calculated Atomization Energies[a] (eV) for Al_2 ($^3\Pi_u$) and Al_3 ($^2A_1'$) and Mean Unsigned Error

	Al_2	Al_3	MUE[b]
B3LYP/6-31+G(d)	1.31	3.19	0.48
B3LYP/MG3	1.35	3.30	0.40
CCSD(T)/6-31+G(d)	1.26	3.35	0.42
CCSD(T)/MG3	1.37	3.62	0.24
experiment[5−7,79,80]	**1.36**	**4.09**	
G3X	1.51	3.84	0.20
MCG3/3	1.45	3.82	0.18
MCG3/3//Qa	1.45	3.82	0.18
MP2/6-31+G(d)	1.18	3.16	0.55
MP2/MG3	1.34	3.43	0.34
MPW1K/6-31+G(d)	1.41	3.42	0.36
MPW1K/MG3	1.46	3.54	0.32
mPW1PW91/6-31+G(d)	1.47	3.61	0.29
mPW1PW91/MG3	1.52	3.73	0.26
PBE0/6-31+G(d)	1.50	3.74	0.24
PBE0/MG3	1.55	3.86	0.21
QCISD/6-31+G(d)	1.18	2.98	0.65
QCISD/MG3	1.26	3.17	0.51

[a] All atomization energies in this article are zero-point exclusive; i.e., they correspond to dissociation from the classical equilibrium structure (this is sometimes called D_e). [b] The MUE is from the experimental atomization energies.

basis set is more affordable than the MG3 basis set. Thus, for larger systems, the geometries for the MCCM/3 calculations will be optimized at the QCISD level with the 6-31+G(d) basis set. It should be noted that the MUE for the QCISD/MG3 geometries (0.008 Å) is similar to the MUE for QCISD/6-31+G(d). The HDFT method with the most accurate bond lengths is MPW1K/MG3, with an MUE of 0.013 Å.

We also report the atomization energies of Al_2 and Al_3 (Table 2). At this point, we have introduced a new notation, //Qa, which means that the energy was calculated with the QCISD/6-31+G(d) geometry. The G3X and MCG3/3 methods agree well with each other for Al_2 and Al_3. The experimental dissociation energies for Al_2 ($^3\Pi_u$) and Al_3 ($^2A_1'$) are 1.34[9] and 2.701[8,10] eV, respectively, where the experimental dissociation energy for Al_3 is the energy required to form infinitely separated Al_2 and Al. Adding the experimental dissociation energies of Al_2 and Al_3 gives the experimental atomization energy of Al_3. These experimental values correspond to 0 K and hence include zero-point energy in the molecules. We calculated the zero point energy from the experimental frequencies (284 cm^{-1} for Al_2[87] and 235 and 360 cm^{-1} for Al_3[88]) and added it to the experimental dissociation energies to produce the experimental zero-point-exclusive atomization energies shown in Table 2. This allows a direct comparison to the calculated results.

The methods with the smallest MUE for atomization energy are MCG3/3, MCG3/3//Qa, and G3X, with MUEs of 0.18, 0.18, and 0.20 eV, respectively. The largest difference between G3X and MCG3/3 is for Al_2, where the calculated atomization energies are 1.51 and 1.45 eV, respectively; the latter is in better agreement with the experimental atomization energy for Al_2 (1.36 eV). Neither MCG3/3 nor G3X agrees well with the experimental atomization energy for Al_3 (4.09 eV); however, this experimental value is suspect because it relies on certain spectroscopic assignments that require further experimental validation. We have therefore chosen MCG3/3 as our preferred multilevel method to calculate the atomization energies for the accurate atomization energies for the small Al data set, because it agrees best with the atomization energy for Al_2. The MCG3/3 method is also more affordable than the G3X method. The CPU time for a single-point energy calculation of Al_3 on an IBM Winterhawk+ computer with a 375 MHz Power3 processor is 16 min with MCG3/3 and 42 min with G3X.

TABLE 3: Atomization Energies (eV) for the Small Aluminum Data Set[a]

	Al_2	Al_3	Al_4	Al_6(opt)	Al_6(bulk)	$Al_7(O_h)$	Al_7(Cs)
B3LYP/6-31+G(d)	1.31	3.19	4.94	9.22	9.07	8.28	12.35
B3LYP/MG3	1.35	3.30	5.09	9.57	9.40	8.79	12.68
MC-CO/2//Qa	1.33	3.35	6.04	12.06	11.54	10.20	15.78
MCG3/3//Qa	1.45	3.82	5.95	11.43	11.32	10.47	15.22
MC-QCISD/3//Qa	1.49	3.90	6.23	11.90	11.79	10.91	15.77
MC-UT/3//Qa	1.43	3.24	5.53	10.57	10.50	10.04	13.98
MPW1K/6-31+G(d)	1.41	3.42	5.35	10.42	10.31	9.10	14.10
MPW1K/MG3	1.46	3.54	5.51	10.83	10.51	9.40	14.42
mPW1PW91/6-31+G(d)	1.47	3.61	5.66	10.82	10.53	9.50	14.53
mPW1PW91/MG3	1.52	3.73	5.81	11.19	10.90	9.78	14.77
PBE0/6-31+G(d)	1.50	3.74	5.85	11.18	10.88	10.13	14.92
PBE0/MG3	1.55	3.86	6.00	11.52	11.27	10.41	15.24

[a] The // qualifier does not apply to the Al_6(bulk) columns of Tables 3 and 4 because the Al_6(bulk) structure is not an optimized structure.

TABLE 4: Mean Errors in the Atomization Energies (eV/atom) for the Small Aluminum Data Set, CPU Time for an Al_7 Calculation, and the Actual or Estimated Time (h) for a Al_{13} Calculation

	MSE[a]	MUE[b]	RMSE[c]	Cost Al_7[d]	Cost Al_{13}[d]
B3LYP/6-31+G(d)	−0.323	0.323	0.374	0.3	3.3
B3LYP/MG3	−0.270	0.270	0.315	9.2	110
MCG3/3//Qa				58.0	837
MC-CO/2//Qa	0.018	0.067	0.078	48.9	644
MC-QCISD/3//Qa	0.066	0.066	0.076	48.5	659
MC-UT/3//Qa	−0.125	0.125	0.144	47.9	635
MPW1K/6-31+G(d)	−0.158	0.158	0.180	0.4	4.4
MPW1K/MG3	−0.114	0.115	0.132	10.3	123
mPW1PW91/6-31+G(d)	−0.101	0.103	0.121	0.3	3.3
mPW1PW91/MG3	−0.056	0.060	0.074	11.6	138
PBE0/6-31+G(d)	−0.042	0.044	0.052	0.3	3.6
PBE0/MG3	0.005	0.011	0.012	10.0	119

[a] Mean signed error as compared to MCG3/3//Qa. [b] Mean unsigned error as compared to MCG3/3//Qa. [c] Root-mean-square error as compared to MCG3/3//Qa. [d] The costs are CPU times for a single-point energy calculation with on an IBM Winterhawk+ computer with a 375 MHz Power3 processor. For consistency, all times over 100 hours are estimated by a consistent scheme in this table (as explained in Supporting Information).

4.2. Small Al Data Set. Table 3 gives the calculated atomization energies for the small Al data set. The mean errors per atom for the atomization energies are given in Table 4 along with computer times. The mean error per atom is defined as the mean error in the seven atomization energies of Table 4 divided by the mean number of atoms in that test set, which is 5.0. The MCCM methods are too costly for a calculation on Al_{13}. We have listed the time for single-point energy calculations of Al_7 and Al_{13} in Table 4. These times are directly calculated when they are under 100 h but otherwise were estimated. For the HDFT/MG3 calculations this involves assuming N^4 scaling, where N is the number of particles; the scheme that was used in estimating the MCCM times is given in Supporting Information, and it assumes no increase in the number of iterations as the number of particle increases. One can see that a single-point energy calculation would take 837 h with MCG3/3 and 119 h with PBE0/MG3. The calculation takes only 3.6 h with PBE0/6-31+G(d), but that would compromise the accuracy. We have actually computed single-point energies for Al_{13} with a few of the more expensive methods in Table 5 and found that the estimated times consistently underestimated the true CPU times, because the number of SCF iterations increases with system size. For example, the time for an Al_{13} calculation with PBE0/MG3 on the same computer was 192 h, which is 73 h longer than what was estimated.

The most accurate HDFT method is PBE0/MG3 with an MUE per atom of 0.01 eV. The most accurate multilevel method

TABLE 5: Bond Lengths (Å) for the Small Aluminum Data Set and the Obtuse Angle (deg) for Al_4

	Al_2	Al_3	$Al_4(R_e)$	$Al_4(\theta_e)$	Al_6(opt)	$Al_7(O_h)$
best estimate[a]	2.709	2.523				
Hybrid Density Functional Theory and QCISD						
B3LYP/6-31+G(d)	2.764	2.544	2.585	111.1	2.749	2.686
B3LYP/MG3	2.752	2.531	2.574	110.8	2.742	2.658
MPW1K/6-31+G(d)	2.716	2.504	2.549	112.6	2.716	2.638
MPW1K/MG3	2.714	2.499	2.545	112.1	2.718	2.623
mPW1PW91/6-31+G(d)	2.734	2.514	2.557	112.3	2.716	2.649
mPW1PW91/MG3	2.729	2.507	2.552	112.0	2.716	2.633
PBE0/6-31+G(d)	2.734	2.513	2.556	112.4	2.713	2.635
PBE0/MG3	2.730	2.506	2.551	112.1	2.714	2.622
QCISD/6-31+G(d)	2.711	2.539	2.578	112.2	2.732	2.641
Semiempirical Methods						
AM1	2.448	2.434	2.392	112.2	2.490	2.393
MNDO	2.381	2.488	2.575	132.7	2.519	2.281
MSINDO	2.413	2.493	2.506	112.5	2.688	2.523
MSINDO/xd	2.488	2.592	2.597	90.2	2.806	2.724
PM3	2.530	2.557	2.568	120.8	2.568	2.616
TBTE	3.104	2.936	2.714	116.9	2.908	2.852

[a] From Table 1.

TABLE 6: Optimized Bond Lengths (Å) for $Al_7(C_s)$

	R_1[a]	R_2[b]	R_3[c]	R_4[d]	R_5[e]	R_6[f]
B3LYP/6-31+G(d)	2.602	2.674	2.601	2.741	2.602	2.969
B3LYP/6-31G(2df,p)	2.600	2.670	2.600	2.734	2.600	2.966
B3LYP/MG3	2.596	2.666	2.595	2.730	2.596	2.962
MPW1K/6-31+G(d)	2.566	2.626	2.565	2.687	2.566	2.893
MPW1K/MG3	2.566	2.623	2.565	2.680	2.566	2.896
mPW1PW91/6-31+G(d)	2.578	2.641	2.577	2.706	2.578	2.908
mPW1PW91/MG3	2.576	2.636	2.575	2.696	2.576	2.910
PBE0/6-31+G(d)	2.576	2.638	2.576	2.704	2.575	2.900
PBE0/MG3	2.575	2.634	2.574	2.695	2.575	2.903
QCISD/6-31+G(d)	2.589	2.651	2.637	2.684	2.637	3.040

[a] Distance between atoms 1 and 7, 5 and 7, and 3 and 7 in Figure 2. [b] Distance between atoms 1 and 2, and 2 and 5 in Figure 2. [c] Distance between atoms 3 and 4, and 3 and 6 in Figure 2. [d] Distance between atoms 2 and 4, 2 and 6, and 3 and 6 in Figure 2. [e] Distance between atoms 1 and 3, and 3 and 5 in Figure 2. [f] Distance between atoms 1 and 6, and 4 and 5 in Figure 2.

(excluding MCG3/3) is MC-CO/3//Qa with an MUE per atom of 0.067 eV. The PBE0/MG3 method is considerably less expensive, however, than any of the multilevel methods (see Table 4). The time for a single-point energy calculation for $Al_7(C_s)$ with the PBE0/MG3 method is 10.0 h, and the time for a single-point energy calculation for $Al_7(C_s)$ with MC-CO/3//Qa is 48.9 h. The time for the same calculation with MCG3/3//Qa is 58.0 h. The least expensive methods are the HDFT methods with the 6-31+G(d) basis set. Unfortunately, reducing the size of the basis set results in a substantially larger error. The most accurate HDFT method with the 6-31+G(d) basis is PBE0, with an MUE per atom of 0.045 eV.

The bond lengths for all of the clusters except $Al_7(C_s)$ are given in the upper section of Table 5, and the bond lengths of $Al_7(C_s)$ are given in Table 6. The HDFT methods have longer bond lengths than the ones computed with QCISD/6-31+G(d). For example, the mean-unsigned difference between PBE0/MG3 and QCISD/6-31+G(d) is 0.035 Å. The HDFT method that agrees best with QCISD/6-31+G(d) is PBE0/6-31+G(d) with a mean unsigned difference of 0.037 Å. This observation had actually been the motivation for including the Al_6(bulk) structure in the small Al data set to test how accurately the HDFT methods agree with MCG3/3 for the same bond length. The PBE0/MG3 method agrees best with the MCG3/3//Qa. The atomization energy for Al_6(bulk) with PBE0/MG3 and MCG3/3//Qa is 11.27 and 11.32 eV, respectively.

5. Large Al Data Set

The atomization energies calculated with the PBE0/MG3 have the best agreement with the atomization energies calculated with MCG3/3, and this method also yields bond distances that are estimated to be typically accurate within a few hundredths of an angstrom. Therefore, we used the PBE0/MG3 method to create a large Al data set consisting mainly of a variety of potential energy curves (PECs) where a PEC is a set of potential energies for a given cluster size that is obtained by varying a single geometrical parameter. The large data set contains twenty PECs for clusters that range in size from Al_2 to Al_7 plus a set of single-point energies for eleven strategically chosen Al_{13} geometries. The twenty PECs involve 179 points and there is a total of 190 points in the large Al data set. In every case we found and used the multiplicity and electronic state symmetry that has the lowest energy for a given point; thus in some cases the PECs contain points of different multiplicity and corresponding to different electronic states. This is one of the aspects of metallic systems that made this study difficult. The Cartesian coordinates and PBE0/MG3 energies of all 190 points are available in the Supporting Information. The multiplicities for PBE0/MG3 and the semiempirical SCF methods are also given in Supporting Information.

5.1. Al_2 and Al_3. There is one PEC for Al_2, and it contains 10 points. For Al_3, there are 6 PECs, which are composed of a total of 57 points: three of these are for Al approaching Al_2 along the C_2-axis, with Al_2 bond lengths of 2.6835, 5.0, and 5.727 Å. Another has Al approaching the dimer's (bond length of 5.727 Å) center of mass at a 45° angle. The fifth has an Al approaching a dimer (bond length of 2.8635 Å) along the dimer's bond axis. The final Al_3 PEC is the breathing motion of the equilateral triangle, where the bond length varies from 2.3 to 3.0 Å.

5.2. Al_4. There are 8 PECs composed of 66 points for Al_4. Three of these PECs have Al approaching equilateral Al_3 (bond length of 2.55 Å). In one the approach is along an on-line C_2-axis to form a rhombus, in another, along the same C_2-axis but from the other direction (toward an vertex), and in the third, along the triangle's C_3-axis to form a tetrahedron. The next three are identical except that the trimer bond length is 2.8635 Å. The final two PECs are for a tetrahedral tetramer isomerizing into a rhombus and for two dimers approaching each other to form a tetrahedron. In the isomerization, one Al moves on a straight-line path into the plane of the other three.

5.3. Al_7. There are 5 PECs composed of 46 points for Al_7. Two of the PECs have Al approaching an octahedron, where the octahedron has a bond length of 2.66 Å; one of these has the approach to a 3-fold site, and the other has the aluminum atom approach to a 2-fold site. A third PEC has Al approaching the 3-fold site again, but with the octahedron, where the octahedron has a bond length of 2.8635 Å. We also have two PECs where a tetrahedron approaches an equilateral triangle (atoms 2, 4, and 6 approaching atoms 1, 3, 5, and 7 in Figure 2). In one PEC, the tetrahedron and triangle have bond lengths of 2.66 Å, and in the other they have a bond length of 2.8635 Å.

5.4. Al_{13}. There are three true Al_{13} structures in the data set. The geometries are face-centered cubic (FCC), hexagonal-close packed (HCP), and icosahedral (see Figure 3). The bond length for the FCC and HCP geometries is 2.8635 Å, and the edge length for the surface of the icoshedron is 2.8635 Å. There is also a set of 8 energies where we begin with the FCC geometry and the atoms are removed one-by-one in different directions, to infinite separation until only eight atoms remain. Thus, for

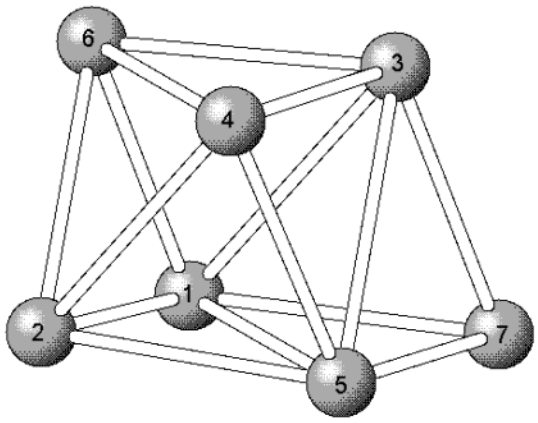

Figure 2. Lowest energy geometry of Al_7.

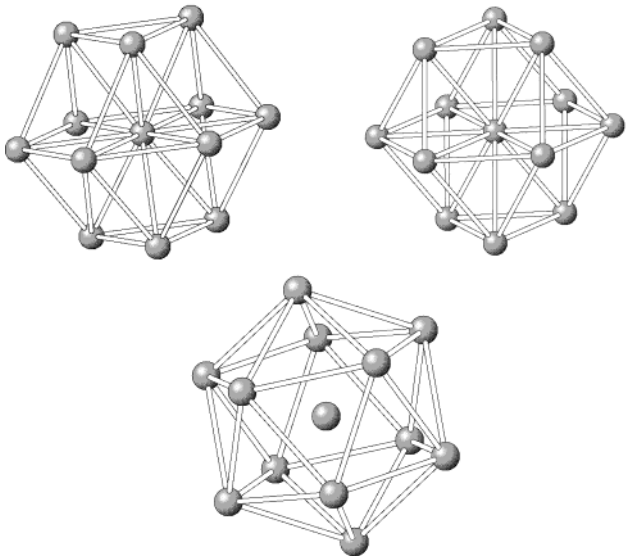

Figure 3. HCP, FCC, and icosahedron structures of Al_{13}.

example, the final Al_{13} system is $Al_8 + 5Al$. It is important to include such structures in the Al_{13} data so that our error function will contain the difference in energy of such a state from the true Al_{13} structures.

6. Cohesive Energies

The cohesive energy is defined as the energy required per atom to dissociate a crystal into infinitely separated neutral atoms; i.e., the cohesive energy is the dissociation energy of a crystal divided by the number of atoms.[89] The cohesive energy can be determined experimentally from the enthalpy of sublimation at 0 K.[90,91] The experimental value is 3.39 eV per atom, which corresponds to dissociation of the solid from its zero-point level. The following paragraph describes the method that we use to remove the zero-point energy (ZPE) from the experimental value, thereby producing a value that can be used to test electronic structure theories.

By making the harmonic approximation for the phonons, the energy of a crystal is given by[92]

$$E_T = U + \int_0^\infty \left(\frac{h\nu e^{-h\nu/kT}}{(1 - e^{-h\nu/kT})} + \frac{h\nu}{2} \right) g(\nu)\, d\nu \qquad (7)$$

where U is the potential energy of the system with atoms at their equilibrium positions, ν is a vibrational frequency, k is Boltzmann's constant, h is Plank's constant, T is temperature, and $g(\nu)$ is a function that gives the number of normal frequencies between ν and $\nu + d\nu$. For 0 K, eq 7 reduces to

$$E_0 = U + \int_0^\infty \left(\frac{h\nu}{2} \right) g(\nu)\, d\nu \qquad (8)$$

U is calculated in an electronic structure calculation, but E_0 is what is determined experimentally. The second term on the right side of eq 8 is the ZPE of a crystal and can be approximated with Debye theory. In this theory,[92]

$$g(\nu)d\nu = \begin{cases} \frac{9N}{\nu_D{}^3}\nu^2\, d\nu & 0 \le \nu \le \nu_D \\ 0 & \nu > \nu_D \end{cases} \qquad (9)$$

where ν_D is the maximum frequency and is called the Debye frequency, and N is the number of atoms. By inserting eq 9 into eq 8 and intergrating, one can obtain

$$E_0 = U + \frac{9}{8} N k \Theta_D \qquad (10)$$

where Θ_D is the Debye temperature defined by[92]

$$\Theta_D = \frac{h\nu_D}{k} \qquad (11)$$

Thus, the ZPE per atom is $9/8k\Theta_D$. The value of Θ_D for aluminum is 428 K,[73] which gives a ZPE of 0.04 eV per atom. Combining this with the enthalpy of sublimation at 0 K yields a zero-point exclusive cohesive energy per atom of

$$\bar{U} = U/N = 3.43 \text{ eV} \qquad (12)$$

This agrees with cohesive energy calculated by Gaudoin et al.[93]

7. Tests of NDO and TB Methods

We tested the six NDO and TB methods against the PBE0/MG3 energies by computing a mean unsigned error (MUE). The MUE was defined by the following function

$$f(X) = \frac{1}{2\bar{N}_{\text{clusters}}} \sum_{k=1}^{k_{\max}} \left(\frac{2}{n_k(n_k-1)} \sum_{i=1}^{n_k-1} \sum_{j=i+1}^{n_k} \left| \Delta\Delta E_{ij}^{kX} \right| + \frac{1}{n_k} \sum_{i=1}^{n_k} \left| \Delta E_i^{kX} \right| \right) \qquad (13)$$

where the sum in k runs over cluster sizes ($k = 1$ for Al_2, 2 for Al_3, 3 for Al_4, 4 for Al_7, and 5 for Al_{13}), n_k is the number of geometries in the data set for the kth cluster, and $f(X)$ is the MUE for a method X, where X is AM1, MNDO, MSINDO, MSINDO/xd, PM3, or TBTE,

$$\bar{N}_{\text{clusters}} = \frac{1}{k_{\max}} \sum_{k=1}^{k_{\max}} N_k \qquad (14)$$

and N_k is the number of atoms in cluster size k. Note that the value of $\bar{N}_{\text{clusters}}$ is 5.8. E_i^k is the ground-state energy for geometry i of Al_k, n_k is the number of geometries of Al_k, $k = 2$, 3, 4, 7, and 13 calculated with PBE0/MG3, and E_i^X is the ground-state energy calculated with AM1, MNDO, MSINDO, MSINDO/xd, PM3, or TBTE,

$$\Delta E_i^{kX} = E_i^k - E_i^X \qquad (15)$$

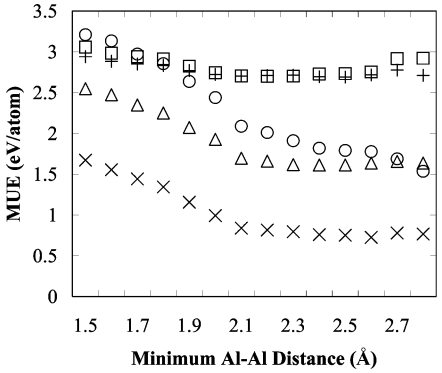

Figure 4. MUE for AM1 (×), MNDO (□), PM3 (+), MSINDO/xd (○), and MSINDO (△) plotted as a function of R_{min}.

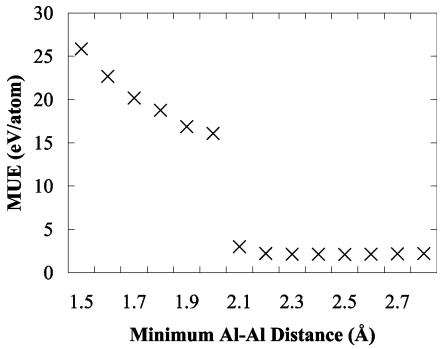

Figure 5. MUE for TBTE (×) plotted as a function of R_{min}.

and

$$\Delta\Delta E_{ij}^{kX} = (E_i^k - E_j^k) - (E_i^X - E_j^X) \qquad (16)$$

Notice that there are five sizes of clusters, and for each size cluster, eq 13 adds the mean unsigned relative error among all pairs of points to the mean unsigned absolute error in binding energy and then divides by 58 to get the MUE per bond. We have adopted this error function so we not only test the atomization energies, but also the local shape of the energy surface.

We also made a subset of the large aluminum data set, called the nonclose Al data set, which removes the points that have small Al−Al distances. This was done because some of the methods perform very poorly in the high-energy regions of the PECs where two or more atoms are close, but there is still an interest in testing them for geometries without close approaches of the atoms because these regions may be unimportant for some applications. The definition to be used for the nonclose Al data set was determined by plotting the MUE as a function of R_{min}, where R_{min} is the minimum Al−Al distance included in the data set (see Figures 4 and 5). As a consequence of the trends in these figures, we have defined the nonclose subset by setting R_{min} equal to 2.25 Å, which removes 38 geometries from the large aluminum data set.

7.1. Al_{13}. The Al_{13} system is especially interesting[94] because it is the smallest cluster in which an Al atom can have a coordination number of 12, which is the value in the close-packed bulk crystal. The results for Al_{13} are shown in Table 7. The results for the FCC structure are in the last column; the FCC structure is a quasispherical cluster carved out of the bulk structure. It is interesting to note that the icosahedron is lower in energy than either of the close-packed structures. Both close-packed[95] and icosahedral[96,97] metal clusters are known from previous work on decorated (i.e., not bare) metal clusters, but there is little known about their systematics. The icosahedral structure has more edges and may therefore be intrinsically more stable; however, one cannot make a periodic bulk structure by repeating icosahedra.

TABLE 7: Atomization Energies (eV) for Al_{13}

	icosahedron	HCP	FCC
AM1	32.08	29.67	29.07
MNDO	17.91	16.73	16.48
MSINDO	23.89	23.66	22.80
MSINDO/x*d*	20.33	23.27	22.28
PBE0/6-31+G(d)	32.10	31.05	30.43
PBE0/MG3[a]	32.55	31.43	30.74
PM3	17.19	17.62	17.70
TBTE	39.02	38.91	38.26

[a] This row is the most reliable result against which the other rows may be tested.

TABLE 8: Mean Unsigned Error (eV/atom) of Six Semiempirical Methods[a]

	AM1	MNDO	MSINDO	MSINDO/xd	PM3	TBTE
large Al data set	0.29	0.53	0.44	0.55	0.51	4.46
nonclose Al data set	0.13	0.46	0.28	0.33	0.47	0.36

[a] Calculated by eq 13.

The most accurate of the NDO and TB methods is AM1; it follows the correct trend in atomization energies of the various Al_{13} structures and has an MUE of 1.29 eV. The TBTE method is the next most accurate method for Al_{13} with an MUE of 3.60 eV, and it also follows the correct trend in atomization energy. The MNDO and MSINDO methods predict the correct trend in atomization energies, but MSINDO/xd and PM3 do not. It is interesting to note that the lack of d functions leads to qualitatively incorrect predictions for the stability of Al_{13} clusters. This is not, however, unsurprising because the MSINDO parameters were determined with d functions.

7.2. AM1, MNDO, MSINDO, MSINDO/xd, and PM3 for the Large Al Data Set. The geometric results for the semiempirical methods are given in the lower part of Table 5. The structures were forced to maintain the same structural symmetry as the optimum geometries for the MCG3/3 calculations; thus for Al_3, Al_4, Al_6(opt), and $Al_7(O_h)$ the geometries are forced to have D_{3h}, D_{2h}, O_h, and O_h symmetry, respectively. The most accurate method for geometries is PM3, with a mean signed difference of 0.08 Å with respect to both QCISD/6-31+G(d) geometries (which were used for the MCG3/3 calculations) and PBE0/MG3 geometries. The worst method is AM1 with a mean signed difference of 0.21 Å with respect to MCG3/3 and 0.19 Å with respect to PBE0/MG3. The AM1, MNDO, MSINDO, and PM3 methods always predict longer bond lengths than the ones from our more accurate calculations. The errors for MSINDO/xd are not as systematic and that method also predicts that Al_4, with D_{2h} symmetry, is nearly square. (It has an obtuse angle of 90.2°.)

The energetic results for the NDO and TB methods are given in Tables 8 and 9. As mentioned earlier, the MUE (obtained from eq 13) may be plotted as a function of R_{min} for MNDO, AM1, MSINDO, MSINDO/xd, and PM3 (see Figure 4). There is a significant improvement in the MUE for AM1, MSINDO, and MSINDO/xd when geometries with small R_{min} are not included. The removal of all 38 points for which any Al−Al distance is less than 2.25 Å decreases the error from 0.29 to 0.13 eV/atom for AM1, from 0.55 to 0.33 for MSINDO/xd, and from 0.44 to 0.28 for MSINDO when the nonclose subset is considered. The error does not decrease as drastically when geometries with small R_{min} are eliminated for the MNDO and PM3 methods. Table 9 shows that when the cluster size increases

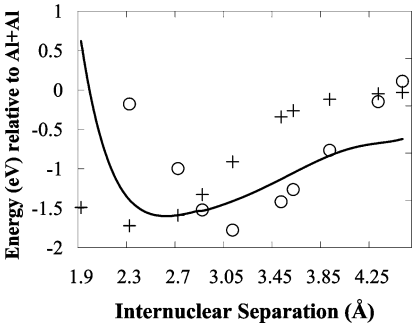

Figure 6. Potential energy curve for Al_2 computed with PBE0/MG3 (line), AM1 (+), and TBTE (○).

TABLE 9: Mean Unsigned Error (eV/atom) for Six Semiempirical Methods as a Function of the Number of Atoms in the Cluster

	N_k	AM1	MNDO	MSINDO	MSINDO/x*d*	PM3	TBTE
large	2	0.34	0.31	0.34	0.31	0.30	1.61
Al data set	3	0.41	0.41	0.35	0.34	0.40	5.03
	4	0.39	0.41	0.39	0.52	0.29	4.23
	7	0.53	0.67	0.77	1.08	0.59	12.62
	13	0.09	0.54	0.31	0.37	0.58	0.43
nonclose	2	0.19	0.22	0.22	0.15	0.22	0.29
Al data set	3	0.19	0.27	0.24	0.20	0.27	0.28
	4	0.19	0.32	0.23	0.27	0.23	0.33
	7	0.16	0.55	0.27	0.39	0.54	0.30
	13	0.09	0.54	0.31	0.37	0.58	0.43

the error becomes worse for MNDO, MSINDO, MSINDO/xd, and PM3, and the errors for AM1 remain fairly constant.

The PEC for Al_2 computed with AM1 and PBE0/MG3 is plotted in Figure 6. The AM1 method, along with MNDO and PM3, was not parametrized for aluminum nanoclusters, but the focus was instead on organoaluminum compounds. Only one pure aluminum compound, Al_2, was used in the parametrization of AM1 and PM3, whereas none were used in the MNDO parametrization. Al_2 was treated incorrectly as a closed-shell singlet in the parametrization of AM1 but was treated more correctly by spin-restricted open-shell Hartree−Fock (ROHF) and taken to be a triplet in the parametrization of PM3. The optimum AM1 bond length for the closed-shell singlet is 2.50 Å, whereas the optimum AM1 bond lengths for an open-shell singlet and triplet are 2.45 and 2.41 Å, respectively. The optimum bond length for PBE0/MG3 is 2.730 Å. The atomization energies for the closed-shell singlet, open-shell singlet, and open-shell triplet are 1.69, 1.82, and 1.80 eV/atom, respectively. Thus, the minimum-energy structure and the repulsive wall for AM1 have both been shifted to the left. One reason for the improvement of AM1 upon deleting the close-contact points is that the PBE0/MG3 energies are repulsive, and strongly repulsive in many cases, for distances less than 2.25 Å, but the AM1 energies are often attractive in that region. The MUE improves significantly because there is such a large difference between the AM1 and PBE0/MG3 energies for points with Al−Al distances less than 2.25 Å. The reason for the large improvement in the results for MSINDO and MSINDO/xd is because the close-contact points for MSINDO and MSINDO/xd are much more repulsive than for PBE0/MG3.

An illustrative example of the problem with close contact points for AM1 is the PEC that has an aluminum atom approaching a dimer (bond length of 2.8635 Å) to form a triangle. In this PEC (Figure 7), the aluminum atom approaches along the dimer's C_2 axis. The corresponding distances of the approaching atom from the center of mass of the dimer are 1.25, 1.9, 2.3, 2.7, 3.1, 3.5, and 3.9 Å. The PEC has 8 geometries,

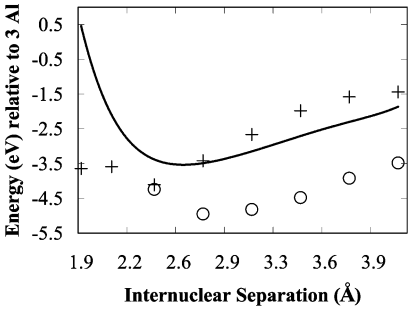

Figure 7. Potential energy curve for Al approaching Al_2 (bond length of 2.8635 Å) along the dimer's C_2-axis computed with the PBE0/MG3 (line), AM1 (+), and TBTE (○) methods.

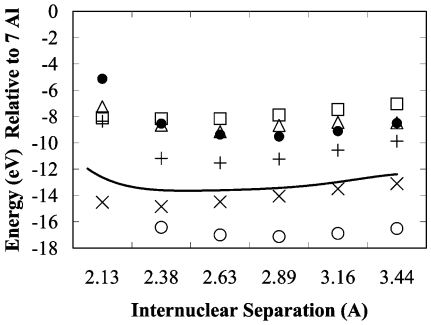

Figure 8. Potential energy curve for Al approaching the 2-fold face of Al_6 (bond length of 2.66 Å) generated with the PBE0/MG3 (line), AM1 (×), MNDO (□), PM3 (△), MSINDO (+), MSINDO/xd (●), and TBTE (○) methods.

and the distance of the approaching Al from either of the atoms of Al_2 is 1.9, 2.07, 2.38, 2.71, 3.06, 3.41, 3.78, and 4.15 Å, respectively. The latter set of distances will be denoted *R*, and this is the axis used for plotting and for discussion. For AM1, the second lowest energy occurs at $R = 1.9$ Å, whereas the $R = 1.9$ Å point is the highest energy structure for PBE0/MG3. One will also notice that the PEC for AM1 is not always smooth; this is because the ground state for the first point, $R = 1.9$, is $^2B_2$, the ground state for the $R = 2.07$, 2.38, 2.71 Å points is $^4A_2$, and the lowest energy state for the remaining points is $^2B_1$. For the PBE0/MG3 PEC, the first three points have a ground state of $^2A_1$, and the remaining points have a ground state of $^4A_2$.

A more typical case is for Al approaching the 2-fold face on an octahedron with a bond length of 2.66 Å. One can see that the MNDO and PM3 results underestimate the binding energy (see Figure 8), and that AM1 agrees well with the PBE0/MG3 results. This PEC is a ridge on the multidimensional potential energy surface, and for the fixed approach it serves as a transition state that connects two minimum energy paths upon which Al approaches a 3-fold face. (The 3-fold face-approach PEC is also present in our data set.) We also have another transition state in the data set, the Al_4 tetrahedron isomerizing into an Al_4 rhombus, where both the rhombus and tetrahedron have bond lengths of 2.5 Å. During the isomerization, three of the atoms remain fixed in the *xz* plane, and the fourth moves on a straight line into that plane. The path for the moving Al atom is $x = x_1 + \lambda(x_2 - x_1)$ and $y = (1 - \lambda)\, y_1$, where x_1, y_1, *z*, and x_2,0, *z* are the initial and final coordinates, respectively, of the fourth atom, and λ is a reaction coordinate that varies from 0 to 1. The two different structures are depicted in Figure 9, and the PEC is given in Figure 10. For this PEC, the MNDO and PM3 methods predict the correct trend and AM1 does not. The AM1 method actually predicts a local minimum near the

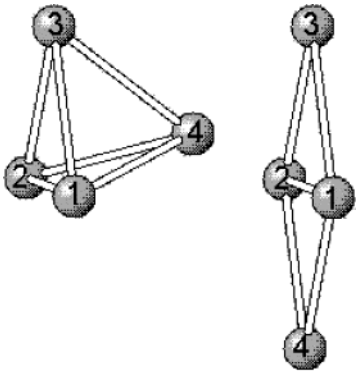

Figure 9. Structures for the Al_4 tetrahedron and rhombus that correspond to $\lambda = 0$ and $\lambda = 1$, respectively, in Figure 10.

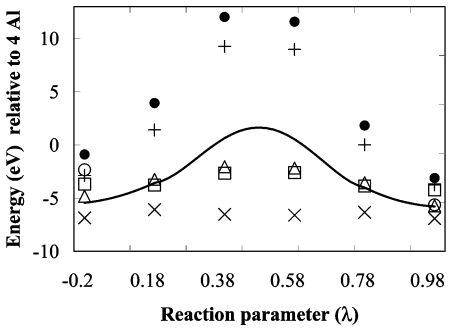

Figure 10. PEC is for an Al_4 tetramer isomerizing into a rhombus. Three atoms are fixed (labeled 1−3) and the fourth atom (labeled 4) moves along a straight line in the *xy*-plane where the coordinates of the fourth atom (x, y, z) are given by $x = x_1 + \lambda(x_2 - x_1)$ and $y = y_1 + \lambda(y_2 - y_1)$, with $z = z_1$, and λ varies from 0 to 1. Results for the PBE0/MG3 (line), AM1 (×), MNDO (□), MSINDO (+),MSINDO/xd (●), PM3 (△), and TBTE (○) methods are shown. The maximum of the accurate curve occurs near $\lambda = 0.5$ at an energy (relative to 4 Al) of 1.6 eV. The data set includes points with $\lambda = 0.0$, 0.2, 0.4, 0.6, 0.8, and 1.0.

transition state. MSINDO and MSINDO/xd also predict the correct trend, but they both predict a much larger barrier.

Another interesting test is to see how often the methods predict the correct multiplicities, where, as for energies, we compare with the PBE0/MG3 results. The multiplicities for PBE0/MG3 and the six semiempirical SCF methods are given in the Supporting Information. The most accurate methods are MSINDO and MSINDO/xd, which predict the correct multiplicity for 68 and 66% of the points, respectively. The worst methods are MNDO and PM3, which predicts the correct multiplicity only 41 and 43% of the time, respectively. AM1 is correct for 49% of the points. For MNDO, 40.5% of the points that do not agree have multiplicities that are less than those obtained with PBE0/MG3, and 18.5% of the points that have multiplicities that are greater than with PBE0/MG3. AM1 makes similar predictions, in that 32% of the points have lower multiplicities, and 19% of the points have greater multiplicities than PBE0/MG3. Similarly, PM3 predicts too low of a multiplicity at 44.5% of the points that do not agree are lower than the correct value, and too high a value at 12.5% of the points. When MSINDO and MSINDO/xd predict the multiplicity incorrectly, they usually predict multiplicities that are smaller than PBE0/MG3. For MSINDO, 29% of the points have lower multiplicities, and 3% have higher. MSINDO/xd is similar with percentages of 28.5 and 5.5, respectively, for the nonclose Al data set. MSINDO and MSINDO/xd are again best; they agree with the PBE0/MG3 results 67 and 66% of the time, respectively, whereas MNDO and PM3 agree only 33 and 42% of the time, and AM1 agrees for 41% of the points. The percentages of points that are above and below the correct value for AM1 are nearly equal for both data sets.

7.3. Tests of the TBTE Method. The geometric results for the TBTE method are given in the lower part of Table 5. The structures, as for the semiempirical methods, were forced to maintain the same structural symmetries as the MCG3/3 calculations. The geometries have a mean unsigned difference of 0.26 Å with respect to QCISD/6-31+G(d) (the geometries used for the MCG3/3 calculations) and 0.28 Å with respect to the PBE0/MG3 geometries. The TBTE methods always predict longer bond lengths than either QCISD/6-31+G(d) or PBE0/MG3.

The MUE for the TBTE energies were calculated with eq 13 and the results are given in Tables 8 and 9. The MUE for the entire data set is quite large, 4.46 eV/atom. However, Figure 5 (discussed above) shows that this large average error is primarily caused by points with Al−Al distances less than 2.25 Å. The method was parametrized against accurate calculations for a variety of crystal structures (body-centered cubic, FCC, HCP, and simple cubic). The minimum Al−Al distance used in the parametrization was 2.645 Å, and the authors warn on their web site (http://cst-www.nrl.navy.mil/bind/al.html) that use of these parameters outside of their parametrization range might result in unphysical energies. We tested this and found that the unphysical energies occur for distances less than 2 Å. We have plotted the PEC for Al_2 (see Figure 6), and the innermost point is not plotted, because it has a value of −17 eV and is off the scale. However, the TBTE method does get the correct dissociation limit. The unphysical energies for small distances are also a limitation for transition states; for example, the TBTE cannot accurately predict the energy of the Al_4 transition state (see Figure 9). The TBTE energies are unphysical (in particular very negative) for all but the end points of the Al_4 isomerization.

The removal of the close contact points reduces the MUE to 0.36 eV/atom, indicating that the TBTE method has reasonable accuracy for clusters with geometries near the equilibrium geometry. In fact, for such geometries, it is more accurate than two of the five more expensive methods (MNDO and PM3). The errors for a given cluster size are given in Table 9. One can see that the errors are larger for the larger clusters, which have more bonds. Nevertheless, the AM1 method is the most accurate of the six inexpensive methods, with respect to energy, for either the full range of geometries or the subset of nonclose ones.

The multiplicities of the TBTE method were always 1 if the system had an even number of Al atoms, and it was 2 if the system had an odd number of Al atoms. These multiplicities agree 35% of the time with the PBE0/MG3 values for the large Al data set and 31% of the time for the nonclose Al data set.

7.4. Cohesive Energies. We calculated the cohesive energy by calculating the binding energy of a large quasispherical cluster and dividing by the total number of atoms in the system. As the clusters get larger, properties should tend to the bulk limit.[97] Using this method, we have calculated the cohesive energy for a number of clusters with the semiempirical methods. The geometries of the quasispherical clusters were determined by constructing a large rectangular FCC lattice and by carving out spheres with an Al atom at the origin. The diameters D of these clusters were calculated by adding the largest Al−Al distance to twice the bulk Al radius; the bulk Al radius is half the Al−Al bulk bond length (1.431 75 Å). The results are in Table 10, and the geometries are available in Supporting

TABLE 10: Cluster Diameter *D* (Å) and Cohesive Energy Calculated with NDO Methods and TBTE for Al_N[a]

		cohesive energy (eV)					
N	*D* (nm)	AM1	MNDO	PM3	MSINDO/x*d*	MSINDO	TBTE
13	7.16	2.23	1.27	1.36	1.71	1.75	2.94
19	9.53	2.46	1.34	1.37	1.83	1.97	3.18
43	11.34	2.74	1.50	1.16	1.71	1.93	3.44
55	12.88	2.81	1.48	1.00	1.61	1.86	3.51
79	14.24						3.71
87	15.46						3.65
135	16.59						3.78
141	17.63						3.79
bulk[b]		3.7	1.9	0.5	1.5	2.1	4.5

[a] The diameter of the quasispherical clusters is taken to be the largest Al−Al distance plus twice the Al−Al bulk radius. [b] Extrapolated by eq 17.

TABLE 11: Mean Unsigned Error Per Atom (eV/atom) for Six Semiempirical Methods[a]

	AM1	MNDO	MSINDO	MSINDO/xd	PM3	TBTE
large Al data set	0.25	0.48	0.41	0.52	0.51	3.74
nonclose Al data set	0.12	0.43	0.27	0.33	0.47	0.33

[a] Calculated by eq 18.

Information. We have estimated the bulk cohesive energy by least-squares fitting the results for the four largest clusters (79−141 for TBTE and 13−55 for the SCF methods) to

$$E_{coh} = E_{coh}^{bulk} - \gamma N^{-1/3} \quad (17)$$

where N is the number of atoms. This assumes an asymptotic $N^{-1/3}$ power law for deviations from the bulk, although one can get reasonable fits with $N^{-2/3}$. The extrapolated values for all methods are given in the last row of Table 10. Comparison to other methods of extrapolation (e.g., using a different set of points or replacing eq 10 by a polynomial in $N^{-1/3}$ or $N^{-2/3}$) shows that the extrapolations are uncertain by at least several tenths of an electron volt, but the results are still useful for drawing conclusions. The method of extrapolation chosen for the table, namely eq 17, is selected simply because it gave the most reasonable set of extrapolations. TBTE predicts a cohesive energy of 4.5 eV and the experimental value is 3.43 eV. Mishin et al.[98] reported that the cohesive energy calculated with the TBTE method is 3.36 eV, which agrees well with the experimental values[99,100] that they obtain from refs 99 and 100. They obtained the value of 3.36 eV, however, by shifting their energies so that the cohesive energy of the minimum energy FCC crystal structure of Al would agree with the experimental cohesive energy. This was done because the STATIC program uses an arbitrary zero of energy.[65]

We have only calculated the cohesive energy for $N = 13$, 19, 43, and 55 for AM1, MNDO, MSINDO, MSINDO/xd, and PM3 methods (Table 11) because the iterative SCF calculations were difficult to converge for larger clusters. Nevertheless, Table 10 shows that only the AM1 method is converging to a reasonable answer. The reader should also keep in mind the difference in costs. For example, for $N = 55$, the AM1 calculation took 1.25 h on an IBM Winterhawk+ computer with a 375 MHz Power3 processor, whereas the TBTE method took 15 s.

7.5. Mean Unsigned Error per Atom. The mean unsigned error per atom is a sensitive function of the size the systems in the test data (larger systems have more bonds and therefore tend to have larger errors). Therefore we computed the mean unsigned error per atom (MUEPA) by the following formula:

$$\mathrm{MUEPA(X)} = \frac{1}{\bar{N}}\frac{1}{6}(5\bar{N}_{clusters} f(X) + \mathrm{UE(CE|X)}) \quad (18)$$

The factor of 5 accounts for the fact that the f(X) function is averaged over 5 cluster sizes; the factor of 6 then averages over these 5 cluster sizes and the unsigned error (UE) in the cohesive energy (CE) for method X (where X is AM1, MNDO, MSINDO, MSINDO/xd, PM3, or TBTE), which is taken as the absolute value of the difference between the extrapolated cohesive energy and 3.43 eV; and $\bar{N}$ is the average number of atoms in each of the six terms:

$$\bar{N} = \frac{5\bar{N}_{clusters} + 1}{6} \quad (19)$$

where $\bar{N}_{clusters}$ is defined above and the second term in the numerator of eq 18 is 1 because the cohesive energy is already on a per-atom basis. Equation 18 yields $\bar{N} = 5$ and the resulting MUEPAs are given in Table 11. AM1 has the smallest error for both the large and the nonclose data sets; the mean unsigned errors per atom for the two data sets are 0.25 and 0.12 eV, respectively.

8. Conclusions

The validation of electronic structure methods has been a difficult task because the reliable experimental data is limited to bulk Al and small systems such as Al_2 and Al_3. Thus, it is difficult to test which methods are reliable for Al nanoparticles. We have thus adopted a bootstrap philosophy in our research. We have begun by calculating the geometries and atomization energies of small Al clusters (Al_2−Al_7) with the highly accurate multicoefficient Gaussian-3 version 3 method (MCG3/3), with which the PBE0 HDFT method with the MG3 basis set agrees to within 0.01 eV per atom for atomization energies and to within a few hundredths of an angstrom for bond lengths. We have also used the PBE0/MG3 method to construct a large and diverse data set of potential energy curves for Al_2, Al_3, Al_4, and Al_7 and 11 energies for Al_{13}. We conclude that the PBE0 hybrid density functional method with the MG3 polarized triple-ζ basis set can be used with reasonable accuracy for Al clusters for which it is affordable (estimated reliability 0.01 eV per atom), but the error increases significantly when the basis set is decreased to a 6-31+G(d) polarized double-ζ set. We have examined several semiempirical methods over the large Al data set, and we find that the most accurate method is AM1 with an MUE per atom, with respect to PBE0/MG3 and the experimental cohesive energy in the bulk, of 0.25 eV/atom, which is further reduced to 0.12 eV if we restrict attention to nonclose points. The MSINDO and TBTE methods, if restricted to geometries without close contacts, also make reasonable predictions for the energies. The MUEs per atom are 0.27 and 0.33 eV, respectively, for geometries without close contacts; however, the TBTE method has an MUE per atom of 3.74 eV/atom if tested over the entire data set. The MUE per atom for MSINDO for the large Al data set is also larger, 0.41 eV/atom, than for the nonclose data set. The TBTE method is significantly less expensive than the other methods tested. The present tests have shown that none of the existing methods has acceptable accuracy for demanding applications, but now that we have an accurate data set for Al_2−Al_{13}, it can be used to develop better methods. Because the MG3 basis set is defined for all elements up to

atomic number 17, the methods in this paper could also be tested for other systems of interest, such as silicon.

Acknowledgment. We are grateful to R. Bruce King and Ahren W. Jasper for helpful discussions and to Mark Mehl for providing the STATIC computer program. This work was supported in part by the Defense University Research Initiative in Nanotechnology (DURINT) through a grant managed by the Army Research Office.

Supporting Information Available: The schemes that we used for estimating the MCCM times are available along with the geometries and PBE0/MG3 energies for the large Al data set, multiplicities for PBE0/MG3, MNDO, AM1, PM3, MSINDO, and MSINDO/xd for the large Al data set, and the geometries of quasispherical clusters. This material is available free of charge via the Internet at http://pubs.acs.org.

References and Notes

(1) *NIST Chemistry Webbook*; Mallard, W. G., Linstrom, P. J., Eds.; NIST Standard Reference Database; NIST: Gaithersburg, MD, 1998; Vol. 69.
(2) Reed, M. A. *Semiconductors Semimetals* **1992**, *35*, 1.
(3) Leskiw, B. D.; Castleman, A. W. J. *Chem. Phys. Lett.* **2000**, *316*, 31.
(4) Leskiw, B. D.; Castleman, A. W. J.; Ashman, C.; Khanna, S. N. *J. Chem. Phys.* **2001**, *114*, 1165.
(5) *Clusters and Nanomaterials*; Kumar, V., Esfarjani, K., Kawazoe, Y., Eds.; Springer: Berlin, 2002.
(6) Coluccia, S.; Gianotti, E.; Marchese, L. *Mater. Sci. Eng. C Biomimetic Supramol. Syst.* **2001**, *15*, 219.
(7) Lee, T.; Liu, J.; Chen, N.-P.; Andres, R. P.; Janes, D. B.; Reifenberger, R. *J. Nanoparticle Res.* **2000**, *2*, 345.
(8) Fu, Z.; Lemire, G. W.; Hamrick, Y. M.; Taylor, S.; Shui, J. C.; Morse, M. D. *J. Chem. Phys.* **1988**, *88*, 3524.
(9) Fu, Z.; Lemire, G. W.; Bishea, G. A.; Morse, M. D. *J. Chem. Phys.* **1990**, *93*, 8420.
(10) Fu, Z.; Russon, L.; Morse, M. D.; Armentrout, P. B. *Int. J. Mass. Spectrom.* **2001**, *204*, 143.
(11) Nyden, M. R.; Petersson, G. A. *J. Chem. Phys.* **1981**, *75*, 1843.
(12) Brown, F. B.; Truhlar, D. G. *Chem. Phys. Lett.* **1985**, *117*, 307.
(13) Gordon, M. S.; Truhlar, D. G. *J. Am. Chem. Soc.* **1986**, *108*, 5412.
(14) Curtiss, L. A.; Raghavachari, K.; Trucks, G. W.; Pople, J. A. *J. Chem. Phys.* **1991**, *94*, 7221.
(15) Montgomergy, J. A.; Ochterski, J. W.; Pettersson, L. G. M. *J. Chem. Phys.* **1994**, *101*, 5900.
(16) Bauschlicher, C. W.; Partridge, H. *J. Chem. Phys.* **1995**, *103*, 1788.
(17) Glukhovtsev, M. N.; Pross, A.; McGrath, M. P.; Radom, L. *J. Chem. Phys.* **1995**, *103*, 1878.
(18) Ochterski, J.; Petersson, G. A.; Montgomergy, J. A. *J. Chem. Phys.* **1996**, *104*, 2598.
(19) Curtiss, L. A.; Raghavachari, K.; Redfern, P. C.; Rassolov, V.; Pople, J. A. *J. Chem. Phys.* **1998**, *109*, 7764.
(20) *Computational Thermochemistry: Prediction and Estimitation of Molecular Thermodynamics*; Irikura, K. K., Frurip, D. J., Eds.; ACS Symposium Series 677; American Chemical Society: Washington, DC, 1998.
(21) Pople, J. A. *Rev. Mod. Phys.* **1999**, *77*, 1267.
(22) Curtiss, L. A.; Redfern, P. C.; Raghavachari, K.; Rassolov, V.; Pople, J. A. *J. Chem. Phys.* **1999**, *110*, 4703.
(23) Fast, P. L.; Corchado, J. C.; Sanchez, M. L.; Truhlar, D. G. *J. Phys. Chem. A* **1999**, *103*, 5129.
(24) Fast, P. L.; Sanchez, M. L.; Corchado, J. C.; Truhlar, D. G. *J. Chem. Phys.* **1999**, *110*, 11679.
(25) Fast, P. L.; Sanchez, M. L.; Truhlar, D. G. *Chem. Phys. Lett.* **1999**, *306*, 407.
(26) Tratz, C. M.; Fast, P. L.; Truhlar, D. G. *PhysChemComm* **1999**, *2*, 14.
(27) Martin, J. M. L.; de Oliveira, G. *J. Chem. Phys.* **1999**, *111*, 1843.
(28) Fast, P. L.; Corchado, J. C.; Sanchez, M. L.; Truhlar, D. G. *J. Phys. Chem. A* **1999**, *103*, 3139.
(29) Vreven, T.; Morokuma, K. *J. Comput. Chem.* **2000**, *21*, 1419.
(30) Curtiss, L. A.; Raghavachari, K.; Redfern, P. C.; Pople, J. A. *J. Chem. Phys.* **2000**, *112*, 1125.
(31) Redfern, P. C.; Zapol, P.; Curtiss, L. A.; Raghavachari, K. *J. Phys. Chem. A* **2000**, *104*, 5850.
(32) Fast, P. L.; Truhlar, D. G. *J. Phys. Chem. A* **2000**, *104*, 6111.
(33) *Quantum-Mechanical Predicition of Thermochemical Data*; Cioslowski, J., Ed.; Understanding Chemical Reactivity Series 22; Kluwer: Dordrecht, The Netherlands, 2001.
(34) Li, Z. H.; Wong, M. W. *Chem. Phys. Lett.* **2001**, *337*, 209.
(35) Curtiss, L. A.; Redfern, P. C.; Rassolov, V.; Kedziora, G.; Pople, J. A. *J. Chem. Phys.* **2001**, *114*, 108.
(36) Curtiss, L. A.; Redfern, P. C.; Raghavachari, K.; Pople, J. A. *J. Chem. Phys.* **2001**, *114*, 9287.
(37) Lynch, B. J.; Truhlar, D. G. *J. Phys. Chem. A* **2002**, *106*, 842.
(38) Curtiss, L. A.; Redfern, P. C.; Raghavachari, K.; Pople, J. A. *Chem. Phys. Lett.* **2002**, *359*, 390.
(39) Lynch, B. J.; Truhlar, D. G. *J. Phys. Chem. A* **2003**, *107*, 3898.
(40) Becke, A. *J. Chem. Phys.* **1993**, *98*, 5648.
(41) Stephens, P. J.; Devlin, F. J.; Chabalowski, C. F.; Frisch, M. J. *J. Phys. Chem.* **1994**, *98*, 11623.
(42) Stephens, P. J.; Devlin, F. J.; Ashvar, C. S.; Bak, K. L.; Taylor, P. R.; Frisch, M. J. *ACS Symp. Ser.* **1996**, *629*, 105.
(43) Adamo, C.; Barone, V. *J. Chem. Phys.* **1998**, *108*, 664.
(44) Adamo, C.; Cossi, M.; Barone, V. *THEOCHEM* **1999**, *493*, 145.
(45) Lynch, B. J.; Fast, P. L.; Harris, M.; Truhlar, D. G. *J. Phys. Chem. A* **2000**, *104*, 4811.
(46) Perdew, J. P.; Wang, Y. *Phys. Rev. B* **1992**, *45*, 244.
(47) Perdew, J. P.; Burke, K.; Ernzerhof, M. *Phys. Rev. Lett.* **1996**, *77*, 3865.
(48) Gordon, M. S.; Binkley, J. S.; Pople, J. A.; Pietro, W. J.; Hehre, W. J. *J. Am. Chem. Soc.* **1982**, *104*, 2797.
(49) Francl, M. M.; Pietro, W. J.; Hehre, W. J.; Binkley, J. S.; Gordon, M. S.; DeFrees, D. J.; Pople, J. A. *J. Chem. Phys.* **1982**, *77*, 3654.
(50) Spitznagel, G. W.; Clark, T.; Schleyer, P. v. R. *J. Comput. Chem.* **1987**, *8*, 1109.
(51) McLean, A. D.; Chandler, G. S. *J. Chem. Phys.* **1980**, *72*, 5639.
(52) Frisch, M. J.; Pople, J. A.; Binkley, J. S. *J. Chem. Phys.* **1984**, *80*, 3265.
(53) Jones, R. O. *J. Chem. Phys.* **1993**, *99*, 1194.
(54) Pettersson, L. G. M.; Bauschlicher, C. W., Jr.; Halicioglu, T. *J. Chem. Phys.* **1987**, *87*, 2205.
(55) Baeck, K. K.; Bartlett, R. J. *J. Chem. Phys.* **1998**, *109*, 1334.
(56) Zhan, C. G.; Zheng, F.; Dixon, D. A. *J. Am. Chem. Soc.* **2002**, *124*, 14795.
(57) Dewar, M. J. S.; Thiel, W. *J. Am. Chem. Soc.* **1977**, *99*, 4899.
(58) Davis, L. P.; Guirdy, R. M.; Williams, J. R.; Dewar, M. J. S.; Rzepa, H. S. *J. Comput. Chem.* **1981**, *2*, 433.
(59) Dewar, M. J. S.; Zoebisch, E. G.; Healy, E. F.; Stewart, J. P. *J. Am. Chem. Soc.* **1985**, *107*, 3902.
(60) Dewar, M. J. S.; Holder, A. J. *Organometallics* **1990**, *9*, 508.
(61) Stewart, J. J. P. *J. Comput. Chem.* **1988**, *10*, 209.
(62) Ahlswede, B.; Jug, K. *J. Comput. Chem.* **1999**, *20*, 563.
(63) Ahlswede, B.; Jug, K. *J. Comput. Chem.* **1999**, *20*, 572.
(64) Cohen, R. E.; Mehl, M. J.; Papaconstantopoulos, D. A. *Phys. Rev. B* **1994**, *50*, 14694.
(65) Mehl, M. J.; Papaconstantopoulos, D. A. *Phys. Rev. B* **1996**, *1996*, 4519.
(66) Yang, S. H.; Mehl, M. J.; Papaconstantopoulos, D. A. *Phys. Rev. B* **1998**, *57*, R2013.
(67) Slater, J. C.; Koster, G. F. *Phys. Rev.* **1954**, *94*, 1498.
(68) Hoffmann, R. *J. Chem. Phys.* **1963**, *39*, 1397.
(69) Hehre, W. J.; Radom, L.; Schleyer, P. v. R.; Pople, J. A. *Ab Initio Molecular Orbital Theory*; Wiley: New York, 1986.
(70) Pople, J. A.; Head-Gordon, M.; Raghavachari, K. *J. Chem. Phys.* **1987**, *87*, 5968.
(71) Rodgers, J. M.; Fast, P. L.; Truhlar, D. G. *J. Chem. Phys.* **2000**, *112*, 3141.
(72) Moore, C. *U.S. Natl. Bur. Stand.* **1952**, Circ. 467.
(73) *American Institute of Physics Handbook*, 3rd ed., Zemansky, M. W., Gray, D. E., Eds.; McGraw-Hill Book Co.: New York, 1972.
(74) Frisch, M. J.; Trucks, G. W.; Schlegel, H. B.; Scuseria, G. E.; Robb, M. A.; Cheeseman, J. R.; Zakrzewski, V. G.; J. A. Montgomery, J.; Stratmann, R. E.; Burant, J. C.; Dapprich, S.; Millam, J. M.; Daniels, A. D.; Kudin, K. N.; Strain, M. C.; Farkas, O.; Tomasi, J.; Barone, V.; Cossi, M.; Cammi, R.; Mennucci, B.; Pomelli, C.; Adamo, C.; Clifford, S.; Ochterski, J.; Petersson, G. A.; Ayala, P. Y.; Cui, Q.; Morokuma, K.; Salvador, P.; Dannenberg, J. J.; Malick, D. K.; Rabuck, A. D.; Raghavachari, K.; Foresman, J. B.; Cioslowski, J.; Ortiz, J. V.; Baboul, A. G.; Stefanov, B. B.; Liu, G.; Liashenko, A.; Piskorz, P.; Komaromi, I.; Gomperts, R.; Martin, R. L.; Fox, D. J.; Keith, T.; Al-Laham, A.; Peng, C. Y.; Nanayakkara, A.; Challacombe, M.; Gill, P. M. W.; Johnson, B.; Chen, W.; Wong, M. W.; Andres, J. L.; Gonzalez, C.; Head-Gordon, M.; Replogle, E. S.; Pople, J. A. *Gaussian98*, version A.11; Gaussian, Inc.: Pittsburgh, PA, 2001.
(75) Rodgers, J. M.; Lynch, B. J.; Fast, P. L.; Zhao, Y.; Pu, J.; Chuang, Y. Y.; Truhlar, D. G. MULTILEVEL-version 3.0.1/G98; University of Minnesota: Minneapolis, MN, 2002.

(76) Stewart, J. J. P.; Rossi, I.; Hu, W. P.; Lynch, G. C.; Liu, Y. P.; Chuang, Y. Y.; Li, J.; Cramer, C. J.; Fast, P. L.; Truhlar, D. G. MOPAC version 5.09mn; Minneapolis, MN, 1999.

(77) Frisch, M. J.; Trucks, G. W.; Schlegel, H. B.; Scuseria, G. E.; Robb, M. A.; Cheeseman, J. R.; Montgomery, J. A., J.; Vreven, T.; Kudin, K. N.; Burant, J. C.; Millam, J. M.; Iyengar, S. S.; Tomasi, J.; Barone, V.; Mennucci, B.; Cossi, M.; Scalmani, G.; Rega, N.; Petersson, G. A.; Nakatsuji, H.; Hada, M.; Ehara, M.; Toyota, K.; Fukuda, R.; Hasegawa, J.; Ishida, M.; Nakajima, T.; Honda, Y.; Kitao, O.; Nakai, H.; Klene, M.; Li, X.; Knox, J. E.; Hratchian, H. P.; Cross, J. B.; Adamo, C.; Jaramillo, J.; Gomperts, R.; Stratmann, R. E.; Yazyev, O.; Austin, A. J.; Cammi, R.; Pomelli, C.; Ochterski, J. W.; Ayala, P. Y.; Morokuma, K.; Voth, G. A.; Salvador, P.; Dannenberg, J. J.; Zakrzewski, V. G.; Dapprich, S.; Daniels, A. D.; Strain, M. C.; Farkas, O.; Malick, D. K.; Rabuck, A. D.; Raghavachari, K.; Foresman, J. B.; Ortiz, J. V.; Cui, Q.; Baboul, A. G.; Clifford, S.; Cioslowski, J.; Stefanov, B. B.; Liu, G.; Liashenko, A.; Piskorz, P.; Komaromi, I.; Martin, R. L.; Fox, D. J.; Keith, T.; Al-Laham, M. A.; Peng, C. Y.; Nanayakkara, A.; Challacombe, M.; Gill, P. M. W.; Johnson, B.; Chen, W.; Wong, M. W.; Gonzalez, C.; Pople, J. A. *Gaussian03*, version A.1; Gaussian Inc.: Pittsburgh, PA, 2003.

(78) Jug, K.; Bredow, T.; Geudtner, G. MSINDO version 2.6. Hannover, Germany, 2003.

(79) Pople, J. A.; Nesbet, R. K. *J. Chem. Phys.* **1954**, *22*, 571.

(80) Mehl, M. J.; Cohen, R. E.; Papaconstantopoulos, D. A. STATIC version 1.11. Washington, DC, 2002.

(81) Cizek, J. *Adv. Chem Phys.* **1969**, *14*, 35.

(82) Purvis, G. D.; Barlett, R. J. *J. Chem. Phys.* **1982**, *76*, 1910.

(83) Raghavachari, K.; Trucks, G. W.; Pople, J. A.; Head-Gordon, M. *Chem. Phys. Lett.* **1989**, *157*, 479.

(84) Raghavachari, K.; Anderson, J. B. *J. Phys. Chem.* **1996**, *100*, 12960.

(85) Bauschlicher, C. W., Jr.; Pettersson, L. G. M. *J. Chem. Phys.* **1987**, *87*, 2198.

(86) Langhoff, S. R.; Bauschlicher, C. W., Jr. *J. Chem. Phys.* **1989**, *92*, 1879.

(87) Cai, M.; Dzugan, T. P.; Bondybey, V. E. *Chem. Phys. Lett.* **1989**, *155*, 430.

(88) Villalta, P. W.; Leopold, D. G. Ph.D. Thesis, University of Minnesota, Minneapolis, 1993.

(89) Kittel, C. *Introduction to Solid State Physics*, 7th ed.; John Wiley & Sons: New York, 1996.

(90) *Selected Values of the Thermodynamic Properties of the Elements*; Hultgren, R., Desai, P. D., Hawkins, D. T., Gleiser, M., Kelly, K. K., Wagman, D. D., Eds.; American Society for Metals: Metals Park, OH, 1973.

(91) Brewer, L. The Cohesive Energy of the Elements. Report 3720; Lawrence Berkeley Laboratory: Berkeley, CA, 1973.

(92) McQuarrie, D. A. *Statistical Mechanics*; University Science Books: Sausalito, CA, 2000.

(93) Gaudoin, R.; Foulkes, W. M. C.; Rajagopal, G. *J. Phys.: Condens. Matter* **2002**, *14*, 8787.

(94) Bauschlicher, C. W., Jr.; Pettersson, L. G. M. *J. Chem. Phys.* **1985**, *84*, 2226.

(95) King, R. B. *Inorg. Chim. Acta* **1986**, *116*, 99.

(96) King, R. B. *Inorg. Chim. Acta* **1996**, *252*, 115.

(97) Lindsay, D. M.; Wang, Y.; George, T. F. *J. Chem. Phys.* **1987**, *86*, 3500.

(98) Mishin, Y.; Farkas, D.; Mehl, M. J.; Papaconstantopoulos, D. A. *Mater. Res. Symp. Proc.* **1999**, *538*.

(99) Wagman, D. D.; Evans, W. H.; Parker, V. B.; Halow, I.; Bailey, S. M.; Schumm, R. H. *Natl. Bur. Stand. (US) Technical Notes 270-3* **1965**.

(100) *CRC Handbook of Physics and Chemistry*, 65th ed.; Weast, R. C., Astle, M. J., Beyer, W. H., Eds.; CRC Press: Boca Raton, FL, 1984.